Supramolecular architectures of molecularly thin yet robust free-standing layers

Moradi, M.; Opara, N.L.; Tulli, L.G.; Wackerlin, C.; Dalgarno, S.J.; Teat, S.J.; ... ; Shahgaldian, P.

APPLIED SCIENCES AND ENGINEERING

Supramolecular architectures of molecularly thin yet robust free-standing layers

Mina Moradi[1,2], Nadia L. Opara[2,3], Ludovico G. Tulli[1], Christian Wäckerlin[4], Scott J. Dalgarno[5], Simon J. Teat[6], Milos Baljozovic[2], Olha Popova[7], Eric van Genderen[2]*, Armin Kleibert[8], Henning Stahlberg[3], Jan Pieter Abrahams[9,10], Celestino Padeste[2], Philippe F.-X. Corvini[1], Thomas A. Jung[2†], Patrick Shahgaldian[1†]

Stable, single-nanometer thin, and free-standing two-dimensional layers with controlled molecular architectures are desired for several applications ranging from (opto-)electronic devices to nanoparticle and single-biomolecule characterization. It is, however, challenging to construct these stable single molecular layers via self-assembly, as the cohesion of those systems is ensured only by in-plane bonds. We herein demonstrate that relatively weak noncovalent bonds of limited directionality such as dipole-dipole (–CN···NC–) interactions act in a synergistic fashion to stabilize crystalline monomolecular layers of tetrafunctional calixarenes. The monolayers produced, demonstrated to be free-standing, display a well-defined atomic structure on the single-nanometer scale and are robust under a wide range of conditions including photon and electron radiation. This work opens up new avenues for the fabrication of robust, single-component, and free-standing layers via bottom-up self-assembly.

INTRODUCTION

The ambition to produce materials with meticulous control over the organization of molecular building blocks has, for decades, attracted chemists and material scientists and triggered their efforts. This long-standing challenge has been met, to a great extent, with the development of reticular chemistry allowing for the design of complex and chemically programmed crystalline materials, namely, metal-organic and covalent-organic frameworks (MOFs and COFs) (*1*, *2*). The strong resurgence of interest in two-dimensional (2D) materials triggered MOF design strategies to be adapted for the production of 2D networks (*3*–*10*). The 2D nature of this class of materials considerably limits their stability; however, a substrate is required. Thus, the possibility to produce stable and, a fortiori, free-standing monolayers remains a challenge. It is remarkable that currently existing methods do not allow for the fabrication of crystalline and free-standing monolayers of organic building units exclusively via supramolecular interactions between their constituent molecules in the absence of chemical linkers. Here, we challenge the accepted paradigm endorsing strong and directional interactions for the design of stable supramolecular architectures: We report a strategy to construct stable and free-standing monomolecular layers using weak noncovalent bonds of limited directionality (i.e., dipole-dipole interactions).

[1]Institute of Chemistry and Bioanalytics, School of Life Sciences, University of Applied Sciences and Arts Northwestern Switzerland, Hofackerstrasse 35, CH-4132 Muttenz, Switzerland. [2]Laboratory for Micro- and Nano-technology, Paul Scherrer Institute, Villigen CH-5232, Switzerland. [3]Center for Cellular Imaging and NanoAnalytics (C-CINA), Biozentrum, University of Basel, Mattenstrasse 26, CH-4058 Basel, Switzerland. [4]Empa–Swiss Federal Laboratories for Materials Science and Technology, CH-8600 Dübendorf, Switzerland. [5]Institute of Chemical Sciences, Heriot-Watt University, Riccarton, Edinburgh, Scotland EH14 4AS, UK. [6]Advanced Light Source, Lawrence Berkeley National Laboratory, 1 Cyclotron Road, MS6R2100, Berkeley, CA 94720, USA. [7]Department of Physics, University of Basel, Klingelbergstrasse 82, 4056 Basel, Switzerland. [8]Swiss Light Source, Paul Scherrer Institute, CH-5232 Villigen, Switzerland. [9]Biozentrum, University of Basel, Switzerland and Laboratory of Biomolecular Research, Paul Scherrer Institute, Villigen, Switzerland. [10]Institute of Biology Leiden, Leiden University, Sylviusweg 72, 2333 BE Leiden, Netherlands.
*Present address: Center for Cellular Imaging and NanoAnalytics (C-CINA), Biozentrum, University of Basel, Mattenstrasse 26, CH-4058 Basel, Switzerland.
†Corresponding author. Email: patrick.shahgaldian@fhnw.ch (P.S.); thomas.jung@psi.ch (T.A.J.)

RESULTS AND DISCUSSION

The design of the molecular building block chosen for our first demonstration of a free-standing layer architecture has been inspired by our previous work on calixarene macrocycles in their function as an organizing molecular entity (*9*). At the phenolic rim of the parent calix[4]arene macrocycle, short alkyl chains were attached to reinforce the hydrophobic character of the amphiphile while preserving its interfacial crystallization propensity. We decided to restrict the work to four-membered ring macrocycles because of their higher level of symmetry and their relative conformational rigidity. To endow this calixarene derivative with the ability to form 2D supramolecular networks, chemical moieties capable of dipole-dipole interactions have been introduced. Methyl-cyano functional groups have been chosen as they have been widely studied for their ability to establish this type of supramolecular interaction (*11*, *12*). 5,11,17,23-tetra-methylcyano-25,26,27,28-tetrapropoxy-calix[4]arene (**1**) was synthesized and fully characterized (see synthesis section in the Supplementary Materials and fig. S1).

The crystallization of **1** from methanol yielded single crystals suitable for x-ray diffraction studies with synchrotron radiation. Inspection of the structure showed that both molecules of **1** are in the pinched-cone conformation and that all methyl-cyano functionalities point away from the calixarene cavities. Symmetry expansion reveals a bilayer system (fig. S2) akin to those found in the vast majority of structures containing *p*-sulfonatocalix[4]arene (*11*, *12*), with hydrophobic layers alternating within the extended structure. The relative conformational flexibility of **1** is likely to be a contributory factor to bilayer formation; examination of the extended structure shows that the symmetry equivalents of **1** pack in an interdigitated manner, forming a series of identifiable CH· · ·N and CH· · ·π interactions (tables S1 to S8).

The formation of layers of **1** at the air-water interface was studied using the Langmuir balance technique and Brewster angle microscopy (BAM; Fig. 1 and table S9). The compression isotherm shows that **1** here forms stable monolayers characterized by a relatively high collapse pressure of 28 mN m^{-1} and a limiting area of 90 $Å^2$ $molecule^{-1}$. It is noteworthy that, unlike the large majority of amphiphilic calixarenes at the air-water interface, the interfacial behavior of **1** displays two main phase transitions at surface pressure values of 3.4 and 17.9 mN m^{-1}

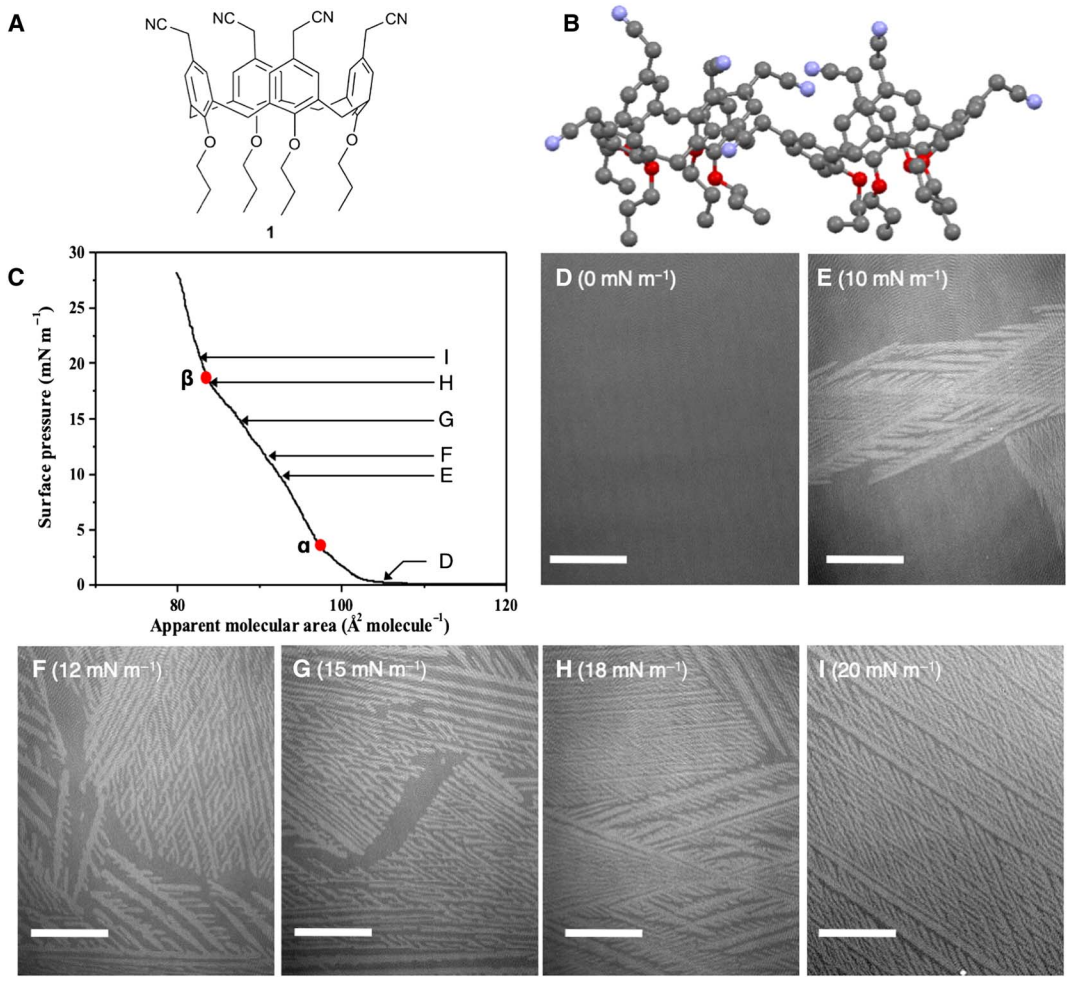

Fig. 1. Chemical structure and interfacial self-assembly characterization of 1. (**A**) Molecular structure of *para*-methyl-cyano-tetra-propoxy-calix[4]arene, **1**. (**B**) Extended structure found in the crystal structure of **1** showing methyl-cyano functionalities pointing away from macrocycle cavities. Color code: C, gray; N, blue; O, red. Hydrogen atoms are omitted for clarity. (**C**) Surface pressure area compression isotherm of **1** on pure water displayed three distinct phases with phase transitions at surface pressure values of 3.4 (α) and 17.9 mN m^{-1} (β), corresponding to molecular area values of 97 and 84 Å^2 molecule^{-1}, respectively. Letter labels indicate the position on the isotherm where the corresponding BAM micrographs were acquired. (**D** to **I**) BAM micrographs of the monolayer of **1** on pure water. Large crystalline monolayer domains grow after the first phase transition (10 mN m^{-1}). Upon further compression, the crystalline network expands and covers the whole available area at the air-water interface. Scale bar, 100 μm.

(Fig. 1, the points labeled α and β on the isotherm, respectively). Before monolayer compression, BAM analysis of the monolayer of **1** at the air-water interface shows no contrast; this is characteristic of a 2D gas phase (Fig. 1D). At the isotherm takeoff (A_0 = 102 Å^2 molecule^{-1}), the monolayer exhibits a homogeneous morphology in BAM (Fig. 1D). After the first phase transition observed at 3.4 mN m^{-1}, the morphology of the monolayer changes to yield large needle-like crystalline structures (Fig. 1, E and F). Upon further compression, the second phase transition is reached; large dendritic crystalline structures appear and gradually cover the whole surface available (Fig. 1, G and H). Further compression increases the density of those crystalline domains (Fig. 1I) until the monolayer collapses.

Notably, BAM results confirm that **1** self-assembles as a crystalline layer at the interface in the absence of organic or inorganic nodes. The addition of transition metal salts (i.e., $CuCl_2$, $NiCl_2$, and $CrCl_3$) did not cause any relevant change in the compression isotherm or BAM micrographs. As cyano moieties are known to be capable of metal coordination, this result strongly suggests that in-layer interactions are largely favored (fig. S3) and that the formation of the crystalline network of **1** is due to intermolecular (–CN· · ·NC–) dipole-dipole interactions. The influence of van der Waals interactions can be neglected because of the short length of aliphatic chains at the lower rim of the macrocycle. To further verify the nature of the intramolecular interaction stabilizing this layer, compression isotherms were carried out in the presence of a competitor molecule capable of (–CN· · ·NC–) interactions, namely, acetonitrile (ACN), in the subphase (fig. S4). The dissociation constant (K_d) of single dipole-dipole interactions, calculated using reported Gibbs' free energy of interaction values (ΔG_0, ranging from −5 to −20 kJ mol^{-1}) of –CN· · ·NC– (*13*), is expected to range from 0.3 to 100 mM. In our experiments, we used ACN concentrations of 10 and 10^{-2} mM. At the lowest tested concentration of 10^{-2} mM (expected to be below K_d), the Langmuir compression isotherm did not reveal any relevant change with regard to that measured on pure water. This confirms that no significant interaction occurred between **1** and ACN. Oppositely, at an ACN concentration of 10 mM, only a very unstable monolayer is formed (with a collapse pressure below 4 mN m^{-1}),

indicating that the interactions of **1** with the cyano group in ACN totally disrupted the self-assembly process. This result further confirms the dipole-dipole nature of the intermolecular forces stabilizing the monolayer of **1**.

The monomolecular layer of **1** was transferred using the Langmuir Schaefer (LS) method at the surface pressure of 20 mN m^{-1} from the air-water interface onto two different solid substrates, i.e., highly oriented pyrolytic graphite (HOPG) and silicon/silicon dioxide coated with octadecyltrichlorosilane (OTS). In both cases, transfer ratio values were close to unity; surface ellipsometry and contact angle measurements confirmed the successful transfer of the monolayer onto the solid substrates tested (table S10). To avoid interferences with the alkyl chains of OTS, HOPG has been chosen as the substrate for surface analytical experiments described hereinafter.

The element-specific chemical analysis of the monolayer of **1** transferred onto HOPG was carried out using x-ray photoelectron spectroscopy (XPS). The N1s spectrum showed only a single peak at 399.7 eV, which is a characteristic value for the cyano CN group attached to carbon (*14*). The single sharp N peak, with a full width at half maximum of 1 eV, provides evidence that all N atoms have the same chemical environment in the monolayer. The O:N ratio, calculated from the O1s and N1s spectra, is ~1, in agreement with the chemical structure of **1**. The amount of water in the transferred monolayer is negligible, as calculated from the O1s spectrum. This provides further counterevidence against H-bonding of **1** with water driving the self-assembly of the monolayer of **1** (Fig. 2, A to C). To further explore whether dipole-dipole interactions between the CN groups are responsible for stabilizing the layer, we transferred the monolayer by LS transfer after assembly on aqueous solutions containing 10 μM $CuCl_2$, $NiCl_2$, or $CrCl_3$ (fig. S3). XPS revealed, in all these cases, the absence of any metal linkers (fig. S5). These results confirm that the CN groups in the calixarene have a higher propensity to interact with one another via dipole-dipole interactions than via coordination bond with metal ion linkers.

To further characterize **1**-based networks transferred on a solid substrate and to establish a molecular model of the monolayer on the surface, near-edge x-ray absorption fine structure (NEXAFS) measurements at the N-K edge were carried out (Fig. 2, D to F). The spectra exhibited a very simple line shape consisting only of the signals of transitions into the π* (400.6 eV) and σ* (approximately 425 eV) molecular orbitals (MOs) of CN (*15*, *16*). Only one peak is observed because the CN MO is not hybridized with the π system of the phenyl group because of the linking sp^3-hybridized carbon (*17*). The linear dichroism (LD) spectrum revealed a slight polarization of the π* signal rising to ~4% at a 70° x-ray incidence angle. The small negative LD implies that, on average, the cyano groups are oriented at an angle γ greater than the magic angle (54.74°) with respect to the surface normal. The angle dependence of the π* LD is modeled as a plane-type orbital (see NEXAFS section in the Supplementary Materials) (*17*, *18*). Also, we find an average angle of the CN group with respect to the surface normal $\langle\gamma\rangle = 57 \pm 1°$.

Atomic force microscopy (AFM) studies of the 2D supramolecular systems provided a substantial challenge; this may be caused by the weak interactions between the short apolar part of **1** (i.e., propyl chains) and the substrate (*19*, *20*). AFM micrographs of the monolayer of **1**, transferred onto HOPG under ambient conditions, were acquired. (Fig. 3). The layer thickness has been determined by measuring the *z* profile after scratching the layer with the AFM at high constant force.

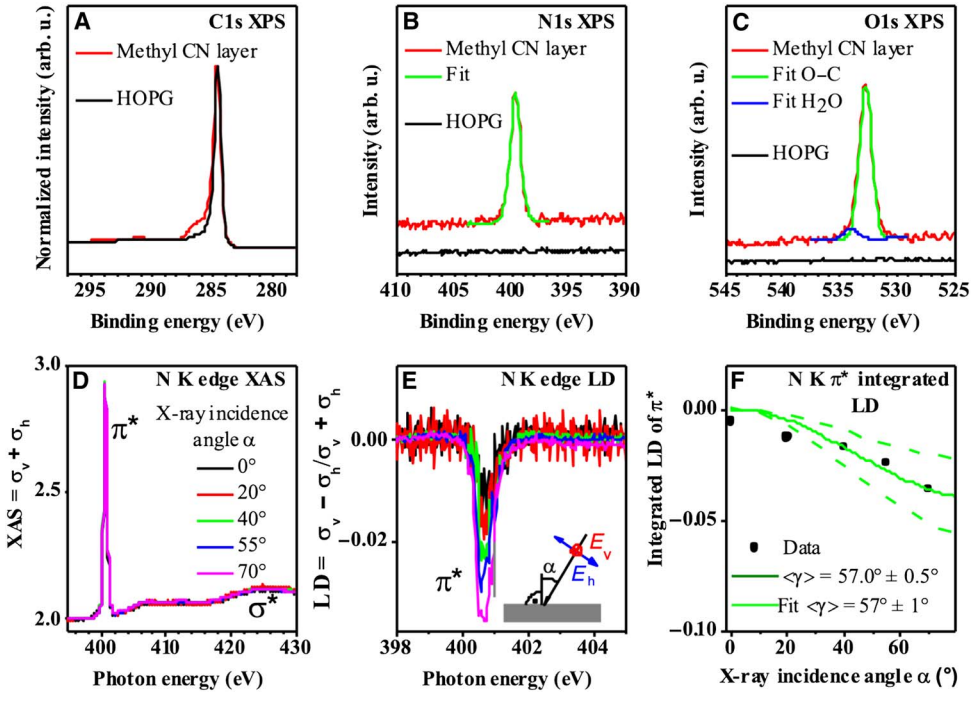

Fig. 2. Surface spectroscopy analysis of 1-based monolayers. (**A** to **C**) X-ray photoelectron spectra of the monolayer of **1** transferred onto HOPG by the LS method for C1s, N1s, and O1s peaks. arb. u., arbitrary units. (C) The O1s spectrum can be fitted with two peaks, 532.5 and 533.2 eV, representing O–C of **1** and an insignificant amount of H_2O (~6% of the O1s spectrum) (*14*). A precise interpretation of the C1s spectrum is challenging because of multiple peaks overlapping for different C entities of **1**. (**D** to **F**) Room temperature N-K edge x-ray absorption spectra ($E_v + E_h$) and LD of the monolayer of **1** on HOPG. (D) The transition into the unoccupied π* MO of the CN groups is visible as a distinct peak at 400.6 eV. (E) Integrated intensity of the LD of the π* signal as a function of the x-ray incidence angle with respect to the surface normal. (F) The data are consistent with an average orientation of $\langle\gamma\rangle = 57°$ of the CN groups. The dashed line corresponds to $\langle\gamma\rangle = 57° \pm 1°$.

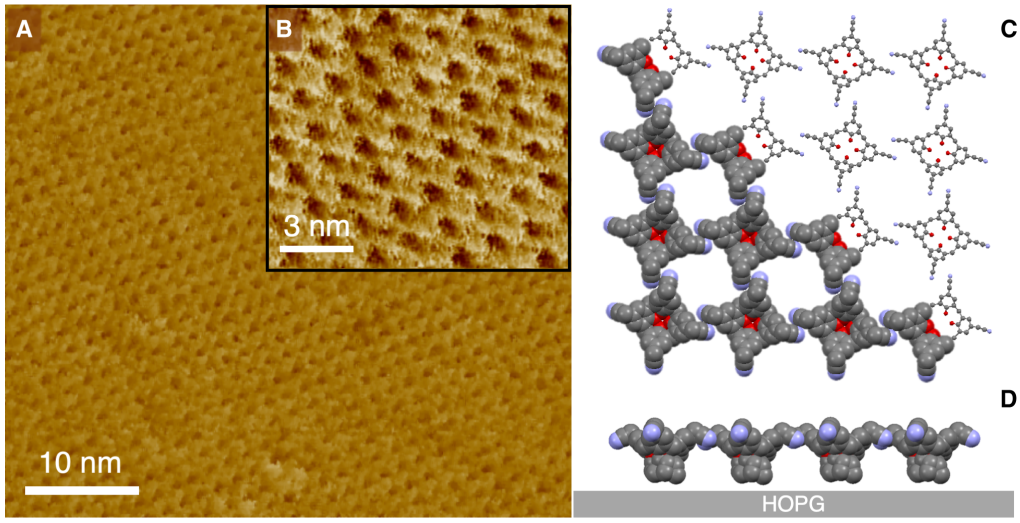

Fig. 3. Molecular resolution AFM imaging of the monolayer of 1. (**A**) AFM images of the monolayer of **1** transferred onto HOPG via the LS method. (**B**) The high-resolution image of the crystalline network of the monolayer shows a highly ordered network formed from the single molecules of **1**. [**C** (top view) and **D** (side view)] Molecular model of the building blocks of **1** interacting via the proposed dipole-dipole interaction in the well-ordered monolayer.

The thereby obtained value of 1.0 ± 0.4 nm further confirms the presence of only a single layer of **1** on HOPG (fig. S6), also consistent with surface ellipsometry measurements that show the value of 1.0 ± 0.2 nm. AFM imaging at molecular resolution revealed large areas covered with molecules of **1** packed in a square fashion with an average lattice constant of 1.5 nm (Fig. 3, A and B). This confirms that the layer is sufficiently stable to be transferred from the liquid to the solid surface without being disrupted by the process despite the above evidenced absence of covalent or coordination bonding.

Combining Langmuir isotherm results, XPS, NEXAFS, and AFM, we propose a model for the molecular packing of **1**-based monolayers (Fig. 3, C and D). In this model, every single building block of **1** interacts with its nearest neighbors via –CN· · ·NC– dipole-dipole interactions. Interatomic distances and angles of the CN groups agree with the values reported by Allen *et al.* (*13*) for dominant antiparallel geometry of dipole-dipole interaction of CN functional groups. The angle of the CN functional groups of **1** with regard to the surface normal, extracted from the molecular model, is 58.4°, which is in agreement with the NEXAFS data.

To further investigate the stability of the layer under different environmental conditions, cryo–transmission electron microscopy (TEM) investigations have been performed on the monolayer of **1** after a successful transfer from the air-water interface onto a lacey carbon copper grid by the LS method (Fig. 4). Lacey carbon grids are hydrophobic by nature and have a mesh structure displaying more than 80% of open areas. The LS transfer was carried out using the same conditions than in the case of HOPG, and the transfer ratio measured was again close to unity. Cryo-TEM investigations of the monolayer of **1**, shown in Fig. 4, revealed the presence of homogeneous free-standing layers across areas as large as 3 μm by 3 μm, without rupturing and shrinking. Thus, the bonding between the molecules in the monolayer is sufficiently stable that it can be transferred as a free-standing film. We attribute this remarkable level of stability to the synergistic action of the dipole-dipole interactions. The diffraction pattern of the free-standing layer shows only one characteristic lattice (Fig. 4B). This, together with the absence of higher-order Laue zones and the high degree of Friedel symmetry in the electron diffraction patterns (also in the shape of the Bragg peaks), confirms that the free-standing layers are indeed monolayers and not ordered or disordered stacks. The electron diffraction patterns of the free-standing monolayer (Fig. 4B) reveal a square lattice with a unit cell size of 15 Å (fig. S7). This result is in agreement with the AFM data and our molecular model.

It has been widely reported that 2D monolayers of organic molecules suffer from decomposition and loss of stability under high electron beam intensity (*21*–*24*). Notably, our results show that the free-standing monolayer of **1** remains intact also during extensive sessions of cryo-TEM imaging.

CONCLUSION

In conclusion, we demonstrated the formation of a crystalline, free-standing supramolecular organic network produced in the absence of coordination or covalent bonds. Thereby, we go beyond the current paradigm endorsing strong and directional interactions for the design of stable supramolecular architectures. The remarkable stability of the layer, despite the absence of covalent bridging of the constitutive building blocks, is reflected in the observation of undistorted free-standing layers and surface-supported layers with the same square crystalline lattice in molecular-resolution AFM and high-resolution TEM, respectively. On the basis of surface chemical analysis and a model, the cohesion between the building blocks of the layer has been attributed to noncovalent dipole-dipole interactions between the functional CN groups of **1**. We expect our chemical design strategy to be versatile so that it could be expanded to a broader range of multivalent building blocks capable of establishing in-plane dipole-dipole interactions. These building blocks should support multiple synergistic dipole-dipole interactions, minimize other less directional interactions such as van der Waals, and form single molecular layers at the solid-liquid interface. The latter is important to gain single molecular layers and not amorphous polymer layers with far less structural and thickness control. The stability of the free-standing layers produced, when exposed to photon-, photoelectron-, and electron irradiations, makes them systems suitable to serve as supporting layers for single-protein and single-nanoparticle analyses and imaging (*25*). Furthermore, the findings reported here pave the way toward the design

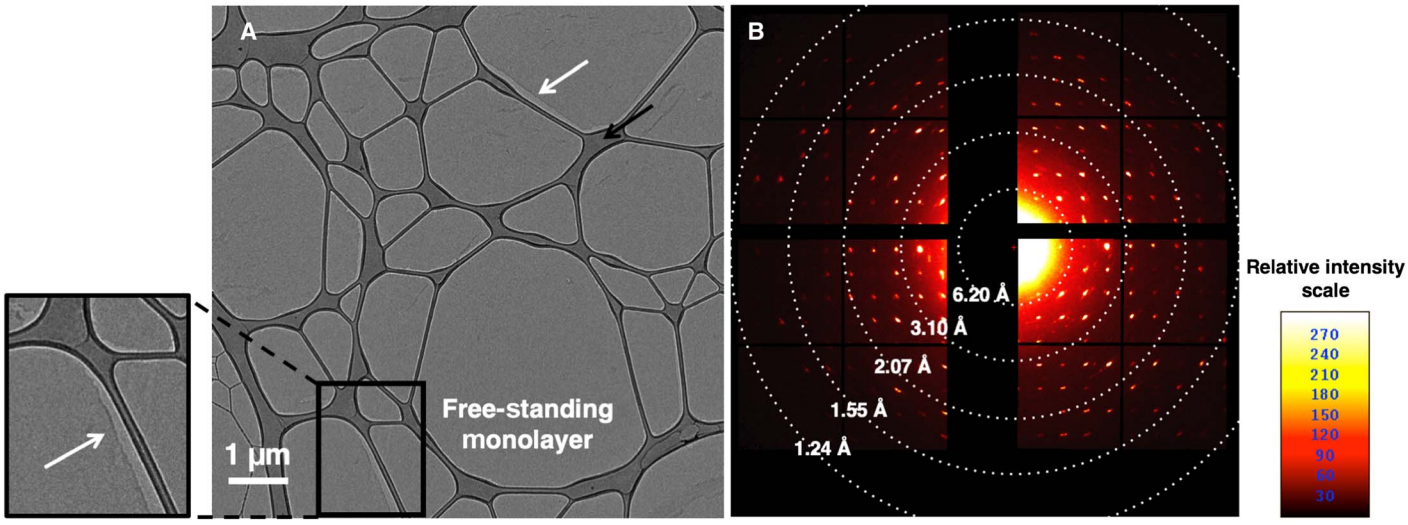

Fig. 4. Cryo-TEM investigation of the free-standing monolayer of 1. (**A**) TEM analysis of the monolayer of **1** transferred via the LS method on a lacey carbon TEM grid [dark areas in the picture are areas of thick carbon from the "lacey carbon" substrate as it is widely used as a TEM substrate for its nonuniform and wide openings (black arrow)]. The layer has fractured and lost contact in some areas with the lacey carbon. In these areas, the free-standing monolayer can be visualized, as shown with white arrows. (**B**) The electron diffraction pattern of the free-standing monolayer of **1** confirms the squarely symmetric packing structure of the crystalline layer. The profile lines across the diffraction pattern (fig. S7) reveal a unit cell size of 15 Å, consistent with the AFM acquired and the molecular model of the self-assembled monolayer of **1**.

of robust 2D layers with molecularly precise architectures and controllable physicochemical properties.

MATERIALS AND METHODS

Synthesis of 5,11,17,23-tetramethylcyano-25,26,27,28-tetrapropoxy calix[4]arene

Compound Cl-C4A-OC_3 (fig. S1) was synthesized as previously described (*26*). 5,11,17,23-tetramethylcyano-25,26,27,28-tetrapropoxy calix[4]arene, **1**, was synthesized using a modified procedure adapted from that described for analogs nonalkylated at phenolic positions (*27*), as follows. Sodium cyanide (0.38 g, 7.63 mmol) was added to a mixture of Cl-C4A-OC_3 (1 g, 1.27 mmol) in dimethyl sulfoxide (150 ml). The reaction mixture was kept under N_2 atmosphere and magnetic stirring at 80°C for 3 hours. The resulting pale yellow solution was cooled down and added to 500 ml of ice/water, yielding a milky solution. This mixture was acidified with an aqueous HCl solution (2 M). The resulting white precipitate was filtered and crystallized from MeOH to yield **1** as white crystals (0.32 g, 34%; mp 200° to 205°C).

^{1}H NMR (nuclear magnetic resonance) (300 MHz, $CDCl_3$): δ 6.62 (s, 2, Ar*H*), 4.45 to 4.41 (d, *J* = 13.3 Hz, 1, Ar-*C*H_2-Ar), 3.87 to 3.81 (t, *J* = 13.3 Hz, 2, O-*C*H_2-CH_2-CH_3), 3.50 (s, 2, Ar-*C*H_2-CN), 3.16 to 3.12 (d, *J* = 13.5 Hz, 1, Ar-*C*H_2-Ar), 1.98 to 1.86 (m, *J* = 7.5 Hz, 2, O-CH_2-*C*H_2-CH_3), and 1.02 to 0.97 (t, *J* = 7.4 Hz, 3, O-CH_2-CH_2-*C*H_3). ^{13}C NMR (75 MHz, $CDCl_3$): δ 156.21, 135.39, 127.81, 123.52, 118.40, 30.87, 23.18, 22.89, 10.26. Mass spectroscopy (electrospray ionization) mass/charge ratio: $[M + Na]^+$, calculated for $[C_{48}H_{52}N_4O_4+Na]^+$ 771.4; found 771.3. Elemental analysis (%) calculated for C, 76.98, H, 7.00; N, 7.48; found, C (76.50, 76.52), H (7.01, 7.05), N (7.42, 7.45).

X-ray crystallography

Data were collected at 100(2) K by shutterless scans using a Bruker D8 diffractometer equipped with a PHOTON 100 detector and operating with a silicon 111 monochromator and synchrotron radiation of wavelength 0.77490 Å. Diffraction data on the crystal powder of **1** were collected using a Bruker D8 Advance powder diffractometer, operating with Ge-monochromated Cu $K_{\alpha 1}$ radiation (wavelength = 1.5406 Å) and a LynxEye linear detector. Data were collected over the angular range of 5° to 85° in 2θ.

Langmuir monolayer, BAM, and LS deposition experiments

Surface pressure area compression isotherms were recorded using a NIMA 112D Langmuir system. For each series of experiments, the trough and barriers were thoroughly cleaned with analytical grade chloroform and nanopure water (resistivity of 18.2 megohm·cm). Nanopure water was used as a subphase. The monolayer was prepared by spreading a solution of **1** (13 μl, 0.5 mg ml^{-1}) in chloroform at the water surface using a gastight microsyringe. After solvent evaporation and equilibration of amphiphiles at the interface (15 min), barriers were symmetrically closed at a speed rate of 5 cm^2 min^{-1}. The accuracies of π_c and A_0 measurements were of ±0.1 mN m^{-1} and ±1 $Å^2$ $molecule^{-1}$, respectively. Each condition was repeated three times to ensure reproducibility of the isotherms.

BAM was performed by using a Nanofilm_ep3 system (Accurion) equipped with an internal solid-state laser at a wavelength of 658 nm. The images were acquired using a charge-coupled device camera (768 × 562 pixels) and a 10× objective, equipped with an automatic focus scanner yielding 1-μm lateral resolution.

LS transfer was carried out using a NIMA deposition system. HOPG and hydrophobic silicon wafers (coated with OTS) (*28*) were used as solid substrates for the LS deposition of the monolayer of **1**. The substrates were brought toward the interface at a controlled speed of 1 mm min^{-1} and touched the monolayer compressed at 20 mN m^{-1}. After 15 min, the substrates were slowly removed from the aqueous solution at a constant speed of 1 mm min^{-1}.

Near-edge x-ray absorption fine spectroscopy

Near edge *X*-ray absorption fine spectroscopy was measured at the N-K edge at room temperature in a total electron yield mode using linearly

polarized x-rays (E_v and E_h) for different incidence angles α (*18*). α = 0° implies normal incidence, E_v is always parallel to the surface plane, and E_h is perpendicular to E_v. The degree of polarization is 100% (*18*). Each spectrum was divided by a matching (same polarization σ and incidence angle α) spectrum obtained on clean HOPG and normalized to unity at the pre-edge (395 to 398 eV).

The angle dependence of the CN π* signal was modeled according to an established procedure (*17*), assuming a plane-type orbital (suitable for the cyano π* MO) for a threefold or higher substrate symmetry. The equations for the intensities I_p and I_n of the absorption, where the electric field of I_n is normal with respect to the surface normal (i.e., in the surface plane) and where I_p is perpendicular to I_n, are as follows

$$I_p = 1 - \cos^2\theta\cos^2\gamma - \frac{1}{2}\sin^2\theta\sin^2\gamma$$
$$I_n = \frac{1}{2}(1 + \cos^2\gamma)$$

Here, γ is the angle between the plane normal to the plane orbital (i.e., the CN vector) and the surface normal, and θ is the angle between the electric polarization of I_p and the surface normal (*17*). The theoretical LD is then calculated as $(I_n - I_p)/(I_n + I_p)$. Note that the photon energy was not exactly calibrated.

SUPPLEMENTARY MATERIALS

Supplementary material for this article is available at http://advances.sciencemag.org/cgi/content/full/5/2/eaav4489/DC1

Section S1. Materials and methods
Section S2. Contact angle measurement
Section S3. Spectroscopic ellipsometry
Section S4. X-ray photoelectron spectroscopy
Section S5. Atomic force microscopy
Section S6. Transmission electron microscopy
Fig. S1. Synthetic route to 5,11,17,23-tetramethylcyano-25,26,27,28-tetrapropoxy calix[4]arene (**1**) and spectroscopic details of **1**.
Fig. S2. X-ray crystal structure determination details of **1**.
Fig. S3. Interfacial properties of the monolayer of **1** in the presence of transition metal ions in the subphase.
Fig. S4. Interfacial properties of the monolayer of **1** in the presence of ACN molecules as competitors with the CN functional groups of **1** for dipole-dipole interactions.
Fig. S5. Surface analysis of the monolayer of **1** in the presence of transition metal ions in the subphase.
Fig. S6. AFM height analysis of the transferred monolayer of **1** from pure water subphase onto HOPG by the LS method.
Fig. S7. Diffraction analysis of the free-standing monolayer of **1** by means of high-resolution cryo-TEM analysis.
Table S1. X-ray crystal structure determination detail of **1**.
Table S2. X-ray crystal structure determination detail of **1**.
Table S3. X-ray crystal structure determination detail of **1**.
Table S4. X-ray crystal structure determination detail of **1**.
Table S5. X-ray crystal structure determination detail of **1**.
Table S6. X-ray crystal structure determination detail of **1**.
Table S7. X-ray crystal structure determination detail of **1**.
Table S8. X-ray crystal structure determination detail of **1**.
Table S9. Characteristic values of the surface pressure-area compression isotherm of **1**.
Table S10. Contact angle measurements on the monolayer of 1 transferred from the air-water interface onto HOPG.
References (*26*–*32*)

REFERENCES AND NOTES

1. H. M. El-Kaderi, J. R. Hunt, J. L. Mendoza-Cortés, A. P. Côté, R. E. Taylor, M. O'Keeffe, O. M. Yaghi, Designed synthesis of 3D covalent organic frameworks. *Science* **316**, 268–272 (2007).
2. M. Eddaoudi, J. Kim, N. Rosi, D. Vodak, J. Wachter, M. O'Keeffe, O. M. Yaghi, Systematic design of pore size and functionality in isoreticular MOFs and their application in methane storage. *Science* **295**, 469–472 (2002).
3. L. Grill, M. Dyer, L. Lafferentz, M. Persson, M. V. Peters, S. Hecht, Nano-architectures by covalent assembly of molecular building blocks. *Nat. Nano.* **2**, 687–691 (2007).
4. L. Lafferentz, V. Eberhardt, C. Dri, C. Africh, G. Comelli, F. Esch, S. Hecht, L. Grill, Controlling on-surface polymerization by hierarchical and substrate-directed growth. *Nat. Chem.* **4**, 215–220 (2012).
5. N. Zhang, T. Wang, X. Wu, C. Jiang, T. Zhang, B. Jin, H. Ji, W. Bai, R. Bai, From 1D polymers to 2D polymers: Preparation of free-standing single-monomer-thick two-dimensional conjugated polymers in water. *ACS Nano* **11**, 7223–7229 (2017).
6. T. Bauer, Z. Zheng, A. Renn, R. Enning, A. Stemmer, J. Sakamoto, A. D. Schlüter, Synthesis of free-standing, monolayered organometallic sheets at the air/water interface. *Angew. Chem. Int. Ed.* **50**, 7879–7884 (2011).
7. K. Baek, G. Yun, Y. Kim, D. Kim, R. Hota, I. Hwang, D. Xu, Y. H. Ko, G. H. Gu, J. H. Suh, C. G. Park, B. J. Sung, K. Kim, Free-standing, single-monomer-thick two-dimensional polymers through covalent self-assembly in solution. *J. Am. Chem. Soc.* **135**, 6523–6528 (2013).
8. A. Shchyrba, C. Wäckerlin, J. Nowakowski, S. Nowakowska, J. Björk, S. Fatayer, J. Girovsky, T. Nijs, S. C. Martens, A. Kleibert, M. Stöhr, N. Ballav, T. A. Jung, L. H. Gade, Controlling the dimensionality of on-surface coordination polymers via endo- or exoligation. *J. Am. Chem. Soc.* **136**, 9355–9363 (2014).
9. M. Moradi, L. G. Tulli, J. Nowakowski, M. Baljozovic, T. A. Jung, P. Shahgaldian, Two-dimensional calix[4]arene-based metal–organic coordination networks of tunable crystallinity. *Angew. Chem. Int. Ed.* **56**, 14395–14399 (2017).
10. R. Dong, T. Zhang, X. Feng, Interface-assisted synthesis of 2D materials: Trend and challenges. *Chem. Rev.* **118**, 6189–6235 (2018).
11. J. L. Atwood, L. J. Barbour, M. J. Hardie, C. L. Raston, Metal sulfonatocalix[4,5]arene complexes: bi-layers, capsules, spheres, tubular arrays and beyond. *Coord. Chem. Rev.* **222**, 3–32 (2001).
12. S. J. Dalgarno, J. L. Atwood, C. L. Raston, Sulfonatocalixarenes: Molecular capsule and 'Russian doll' arrays to structures mimicking viral geometry. *Chem. Commun.* 4567–4574 (2006).
13. P. A. Wood, S. J. Borwick, D. J. Watkin, W. D. S. Motherwell, F. H. Allen, Dipolar C≡N…C≡N interactions in organic crystal structures: Database analysis and calculation of interaction energies. *Acta Cryst.* **B64**, 393–396 (2008).
14. J. F. Moulder, W. F. Stickle, P. E. Sobol, K. D. Bomben, *Handbook of X-ray Photoelectron Spectroscopy*, J. Chastain, Ed. (Perkin-Elmer Corporation Physical Electronics Division, 1992).
15. A. Chernenkaya, K. Medjanik, P. Nagel, M. Merz, S. Schuppler, E. Canadell, J.-P. Pouget, G. Schönhense, Nature of the empty states and signature of the charge density wave instability and upper Peierls transition of TTF-TCNQ by temperature-dependent NEXAFS spectroscopy. *Eur. Phys. J. B.* **88**, 13 (2015).
16. S. Yu, S. Ahmadi, M. Zuleta, H. Tian, K. Schulte, A. Pietzsch, F. Hennies, J. Weissenrieder, X. Yang, M. Göthelid, Adsorption geometry, molecular interaction, and charge transfer of triphenylamine-based dye on rutile TiO_2(110). *J. Chem. Phys.* **133**, 224704 (2010).
17. J. Stöhr, *NEXAFS Spectroscopy* (Springer Series in Surface Sciences, Springer, ed. 1, 1996).
18. U. Flechsig, F. Nolting, A. Fraile Rodríguez, J. Krempaský, C. Quitmann, T. Schmidt, S. Spielmann, D. Zimoch, Performance measurements at the SLS SIM beamline. *AIP Conf. Proc.* **1234**, 319–322 (2010).
19. M. Pfeffermann, R. Dong, R. Graf, W. Zajaczkowski, T. Gorelik, W. Pisula, A. Narita, K. Müllen, X. Feng, Free-standing monolayer two-dimensional supramolecular organic framework with good internal order. *J. Am. Chem. Soc.* **137**, 14525–14532 (2015).
20. Q. An, Q. Chen, W. Zhu, Y. Li, C.-a. Tao, H. Yang, Z. Li, L. Wan, H. Tian, G. Li, A facile method for preparing one-molecule-thick free-standing organic nanosheets with a regular square shape. *Chem. Commun.* **46**, 725–727 (2010).
21. W. Bai, Z. Jiang, A. E. Ribbe, S. Thayumanavan, Smart organic two-dimensional materials based on a rational combination of non-covalent interactions. *Angew. Chem. Int. Ed.* **55**, 10707–10711 (2016).
22. I. Müllerová, M. Hovorka, L. Frank, A method of imaging ultrathin foils with very low energy electrons. *Ultramicroscopy* **119**, 78–81 (2012).
23. R. Dong, M. Pfeffermann, H. Liang, Z. Zheng, X. Zhu, J. Zhang, X. Feng, Large-area, free-standing, two-dimensional supramolecular polymer single-layer sheets for highly efficient electrocatalytic hydrogen evolution. *Angew. Chem. Int. Ed.* **54**, 12058–12063 (2015).
24. D. Zhang, Y. Zhu, L. Liu, X. Ying, C.-E. Hsiung, R. Sougrat, K. Li, Y. Han, Atomic-resolution transmission electron microscopy of electron beam–sensitive crystalline materials. Science **359**, 675–679 (2018).
25. J. Miao, T. Ishikawa, I. K. Robinson, M. M. Murnane, Beyond crystallography: Diffractive imaging using coherent x-ray light sources. *Science* **348**, 530–535 (2015).
26. M. H. Düker, R. Gómez, C. M. L. Vande Velde, V. A. Azov, Upper rim tetrathiafulvalene-bridged calix[4]arenes. *Tetrahedron Lett.* **52**, 2881–2884 (2011).

27. C. D. Gutsche, K. C. Nam, Calixarenes. 22. Synthesis, properties, and metal complexation of aminocalixarenes. *J. Am. Chem. Soc.* **110**, 6153–6162 (1988).
28. N. Moridi, C. Wäckerlin, V. Rullaud, R. Schelldorfer, T. A. Jung, P. Shahgaldian, Langmuir–Blodgett monolayer stabilization using supramolecular clips. *Chem. Commun.* **49**, 367–369 (2013).
29. X. Llopart, R. Ballabriga, M. Campbell, L. Tlustos, W. Wong, Timepix, a 65k programmable pixel readout chip for arrival time, energy and/or photon counting measurements. *Nucl. Instr. Meth. Phys. Res. A* **581**, 485–494 (2007).
30. E. van Genderen, M. T. B. Clabbers, P. P. Das, A. Stewart, I. Nederlof, K. C. Barentsen, Q. Portillo, N. S. Pannu, S. Nicolopoulos, T. Gruene, J. P. Abrahams, Ab initio structure determination of nanocrystals of organic pharmaceutical compounds by electron diffraction at room temperature using a Timepix quantum area direct electron detector. *Acta Cryst. A* **72**, 236–242 (2016).
31. M. T. B. Clabbers, E. van Genderen, W. Wan, E. L. Wiegers, T. Gruene, J. P. Abrahams, Protein structure determination by electron diffraction using a single three-dimensional nanocrystal. *Acta Cryst.* **D73**, 738–748 (2017).
32. K. Suwinska, O. Shkurenko, C. Mbemba, A. Leydier, S. Jebors, A. W. Coleman, R. Matar, P. Falson, Trianionic calix[4]arene monoalkoxy derivatives: Synthesis, solid-state structures and self-assembly properties. *New J. Chem.* **32**, 1988–1998 (2008).

Acknowledgments: We thank R. Schelldorfer for technical support for XPS and AFM measurements and M. Clabbers for the electron diffraction data conversion (from the direct electron detector format). Part of this work was performed at the Surface/Interface: Microscopy (SIM) beamline of the Swiss Light Source, Paul Scherrer Institute, Villigen, Switzerland. **Funding:** The financial support of the Swiss Nanoscience Institute (grant nos. P1305 and P1308) is gratefully acknowledged. C.W. acknowledges financial support by the University Research Priority Program LightChEC of the University of Zürich, Switzerland. M.B. and T.A.J. acknowledge the Swiss National Science Foundation (grant nos. 200020-153549, 200020-175800, and 206021-113149). This research used resources of the Advanced Light Source, which is a DOE Office of Science User Facility under contract no. DE-AC02-05CH11231. This research was in part supported by the SNF [grant no. 5204.23000.160.02; "SwissFEDI, a free electron diffraction instrument for nano-diffraction of biological specimens" (2016–2019) to J.P.A.]. **Author contributions:** P.S. and T.A.J. conceived the research. M.M. and L.G.T. performed LB, BAM, LS, contact angle, ellipsometry, and AFM experiments and analyzed the data. M.M. and M.B. conducted XPS experiments and analyzed the data. N.L.O. and E.v.G. performed EM data collection, with H.S., J.P.A., and C.P. interpreted the data. L.G.T. and M.M. synthesized the molecule. C.W., M.B., O.P., and A.K. acquired the NEXAFS data and analyzed the data. S.J.D. and S.J.T. performed the single-crystal x-ray diffraction work. M.M., T.A.J., P.F.-X.C., and P.S. wrote the paper. All authors commented on the manuscript. **Competing interests:** The authors declare that they have no competing interests. **Data and materials availability:** All data needed to evaluate the conclusions in the paper are present in the paper and/or the Supplementary Materials. Additional data related to this paper may be requested from the authors. Crystallographic data for the structure of compound **1**, reported in the Supplementary Materials, have been deposited at the Cambridge Crystallographic Data Centre under deposition no. CCDC 1586569. Copies of the data can be obtained free of charge at www.ccdc.cam.ac.uk/data_request/cif.

Submitted 17 September 2018
Accepted 11 January 2019
Published 22 February 2019
10.1126/sciadv.aav4489

Citation: M. Moradi, N. L. Opara, L. G. Tulli, C. Wäckerlin, S. J. Dalgarno, S. J. Teat, M. Baljozovic, O. Popova, E. van Genderen, A. Kleibert, H. Stahlberg, J. P. Abrahams, C. Padeste, P. F.-X. Corvini, T. A. Jung, P. Shahgaldian, Supramolecular architectures of molecularly thin yet robust free-standing layers. *Sci. Adv.* **5**, eaav4489 (2019).

ScienceAdvances

Supramolecular architectures of molecularly thin yet robust free-standing layers

Mina Moradi, Nadia L. Opara, Ludovico G. Tulli, Christian Wckerlin, Scott J. Dalgarno, Simon J. Teat, Milos Baljozovic, Olha Popova, Eric van Genderen, Armin Kleibert, Henning Stahlberg, Jan Pieter Abrahams, Celestino Padeste, Philippe F.-X. Corvini, Thomas A. Jung, and Patrick Shahgaldian

Sci. Adv., **5** (2), eaav4489.
DOI: 10.1126/sciadv.aav4489

Science Advances (ISSN 2375-2548) is published by the American Association for the Advancement of Science. 1200 New York Avenue NW, Washington, DC 20005. The title *Science Advances* is a registered trademark of AAAS.